American Mineralogist, Volume 88, pages 1718–1723, 2003

Crystal structure of protoanthophyllite: A new mineral from the Takase ultramafic complex, Japan

HIROMI KONISHI,[1,*] THOMAS L. GROY,[2] ISTVÁN DÓDONY,[2,3] RITSURO MIYAWAKI,[4] SATOSHI MATSUBARA,[4] AND PETER R. BUSECK[1,2]

[1]Department of Geological Sciences, Arizona State University, Tempe, Arizona 85287-1404, U.S.A.
[2]Department of Chemistry/Biochemistry, Arizona State University, Tempe, Arizona 85287-1604, U.S.A.
[3]Department of Mineralogy, Eötvös L. University, Budapest, H-1117, Pázmány Péter sétány 1/C, Hungary
[4]Department of Geology, National Science Museum, 3-23-1 Hyakunincho, Shinjuku, Tokyo 169-0073, Japan

ABSTRACT

Protoanthophyllite, $(Mg, Fe)_7Si_8O_{22}(OH)_2$, is a newly discovered amphibole species from the Takase ultramafic complex in Japan. It occurs as prismatic crystals up to 5 mm in length in a thermally altered serpentinite that experienced contact metamorphism. The protoanthophyllite is associated with forsterite, talc, serpentine minerals, chlorite, chromian spinel, magnetite, pentlandite, and calcite. Some protoanthophyllite crystals contain minute lamellae of anthophyllite, other pyriboles, or both. Protoanthophyllite is biaxial negative, with refractive indices n_α = 1.593(2), n_β (calc.) = 1.609, n_γ = 1.615(2), and $2Vx$ = 64(5)°. Electron microprobe analyses give an empirical formula of $(Mg_{6.31}Fe_{0.61}Na_{0.06}Mn_{0.01}Ni_{0.01})_{\Sigma 7.00}(Si_{7.90}Al_{0.14})_{\Sigma 8.04}O_{22}(OH)_2$. It is orthorhombic with space group *Pnmn*. The unit-cell dimensions are a = 9.3553(8), b = 17.9308(15), and c = 5.3117(4) Å: with V = 891.0(3) Å^3 and Z = 2. A single-crystal X-ray structure determination shows that, following the convention of Thompson (1981), protoanthophyllite has an (X) configuration. The topology of the silicate tetrahedral chains is similar to that of the anthophyllite A-chains. Silicate tetrahedral chains are O-rotated in protoanthophyllite, whereas those in protoferro-anthophyllite are S-rotated. Iron atoms are concentrated in the 4-coordinated M4 sites. The unit-cell volume is ~1.5% larger than the equivalent volume of anthophyllite with Mg/(Mg + Fe) = 0.885, suggesting a high-temperature or low-pressure stability relative to anthophyllite, assuming that protoanthophyllite is not metastable.

INTRODUCTION

The *Pnmn* amphibole structure was first identified in synthetic Li-, F-, Mg-bearing and Li-, F-, Fe-, Mn-bearing specimens, and the crystal structure was refined (Gibbs et al. 1960; Gibbs 1969 and personal communication). It is structurally related to orthoamphibole in the same way that protoenstatite (Smith 1959) is related to enstatite, as predicted by Gibbs et al. (1960), who called it protoamphibole. Octahedral layers in amphibole, like in other pyriboles, have two orientations related by a half-rotation about the **b**-axis. A cross (X) refers to a half-rotation between successive octahedral layers whereas a dot (•) refers to no rotation (Thompson 1970, 1981). *Pnmn* amphibole, like protoenstatite, has an (X) configuration whereas *Pnma* amphibole, like enstatite, has a (•X) configuration. Hence, the terms proto and ortho refer to (X) and (•X) configurations, respectively.

The first natural protoamphiboles (Sueno et al. 1998) were not reported until almost 40 years later than the paper by Gibbs et al. (1960). Fe-species (protoferro-anthophyllite) occurs in pegmatites, and Fe-, Mn-species (protomangano-ferro-anthophyllite) occurs in both pegmatites and a metamorphosed manganese deposit. Subsequently, we discovered the Mg-, Fe-species of protoamphibole (protoanthophyllite) from three metamorphosed serpentinites in Japan (Konishi et al. 2002). Here, we present the results of the structural refinement of protoanthophyllite from the Takase ultramafic complex.

The mineral and mineral name of protoanthophyllite have been approved by the Commission on New Minerals and Mineral Names of the International Mineralogical Association (no. 2001-065). The mineral is named after the proto-type analogue of anthophyllite, following the report of amphibole nomenclature by Leake et al. (1997). Type material is preserved at the National Science Museum, Tokyo, Japan, and the Smithsonian Institution, Washington, D.C.

EXPERIMENTAL METHODS

Single-crystal X-ray intensity data were collected using a Bruker SMART APEX CCD diffractometer at Arizona State University. A crystal fragment, free of {100} and {010} lamellae, was selected and cut from a petrographic thin section for the X-ray measurement. We used the SMART V5.622 system of programs for unit-cell determination and X-ray data collection, SAINT V6.02A

*Present Address: Department of Earth and Planetary Sciences, The University of New Mexico, Albuquerque, NM 87131-1116, U.S.A. E-mail: hkonishi85282@hotmail.com

for unit-cell refinement and data reduction, SHELXS97 (Sheldrick 1997b) for the structure solution, and SHELXL97 (Sheldrick 1997a) for refinement. The populations of the coordination polyhedra containing the M cations were refined allowing for Mg and Fe summing to full occupancy. We tried to refine the structure assuming that Al occupies both T and M sites, but the resulting populations of Al on M sites were very small or negative numbers. Therefore, we assumed that the Al occupies only T sites, and the populations on the T sites were refined allowing for Si and Al summing to full occupancy. We constrained the number of Na atoms to equal that of Al. Table 1 gives the details of the collection and refinement.

The compositions of individual crystals were determined using electron microprobe analyses with a JEOL JXA-8600SX instrument at Arizona State University using wavelength-dispersive spectroscopy at an accelerating voltage of 15 kV, a 10 nA beam current, and a ~1 μm beam diameter. Data reduction was done using standard ZAF matrix correction procedures. The following natural and synthetic standards were used: hypersthene for Si, rutile for Ti, anorthite for Al, chromite for Cr, fayalite for Fe, rhodonite for Mn, metallic Ni for Ni, forsterite for Mg, wollastonite for Ca, albite for Na, and orthoclase for K.

TABLE 1. Crystal data and results of structure refinement of protoanthophyllite

Crystal Data	
Crystal system	Orthorhombic
Space group	*Pnmn*
Cell parameters	a = 9.3553(8), b = 17.9308(15), c = 5.3117(4) Å
	Cell parameters from 2459 reflections
Volume	891.0(3) Å^3
Z	2
Dx	2.982 g/cm3
Crystal	0.07 × 0.07 × 0.04 mm^3
	Cleaved fragment, colorless
Cell measurement temperature	293(2) K
Cell measurement θ_{min}	2.27
Cell measurement θ_{max}	29.99
Data Collection	
Radiation type	Mo*Kα*
Radiation source	Fine-focus sealed tube
Data collection wavelength (Å)	0.71073
Monochromator	Graphite
Measurement method	ω scan
Absorption correction type	Empirical
Absorption correction details	Bruker SADABS
Minimum transmission T_{min}	0.7844
Maximum transmission T_{max}	0.9231
Measured reflections	9680
Independent reflections	1348
Reflections with $I>2\sigma(I)$	961
θmin	2.27
θmax	30
Miller index limits	h = –13 to +13
	k = –25 to +25
	l = –7 to +7
Refinement	
Refinement on F^2	
Structure factors for least-squares	Fsqd
Least-squares derivatives matrix	Full
Weighting scheme for least-squares	Calc
Weighting scheme details	
calc w = $1/[\sigma^2(F_o^2)+(0.0437P)^2+0.0000P]$ where $P = (F_o^2+2F_c^2)/3$	
$R[F^2>2\sigma(I)]$	0.0471
$wR(F^2)$	0.1013
Goodness of Fit (S)	0.985
Refl. used in L.S. derivatives	1348
Parameters refined	111
Number of restraints	12
Primary structure solution	Direct
Secondary structure solution	Difmap
Hydrogen sites solution	Geom
Hydrogen sites refinement	Mixed
(Δ/σ)max	0.002
$\Delta\rho_{max}$ (Å^{-3})	0.903
$\Delta\rho_{min}$ (Å^{-3})	–0.725

The optical properties were measured using a polarizing microscope with a universal stage. The indices of refraction (n_α and n_γ) were measured by the immersion method in white light. From these data, the index n_β was calculated.

SAMPLE DESCRIPTIONS

A drill-core sample was collected from a waste dump at the closed Takase chromite mine in the Takase ultramafic complex, Okayama Prefecture, Japan (35° N, 133°20' E). The sample consists of protoanthophyllite, forsterite, talc, serpentine minerals, chlorite, chromian spinel, magnetite, pentlandite, and calcite. The protoanthophyllite occurs as prismatic crystals less than 5 mm in length along the **c**-axis. Some protoanthophyllite crystals include minute lamellae of anthophyllite on {100}, other pyriboles on {010}, or both.

The Takase ultramafic complex experienced contact metamorphism through the intrusion of Cretaceous or Paleogene granitic rocks, and has crystallized to critical mineral assemblages of (1) forsterite + talc ± tremolite, (2) forsterite + anthophyllite ± tremolite, or (3) forsterite + enstatite ± tremolite (Matsumoto et al. 1995). The assemblages are similar to those described by Evans and Trommsdorff (1970) in the Central Alps. Based on the minerals in the drill-core sample, it is most likely from zone 2. Protoanthophyllite may have formed by either the reaction: 4 forsterite + 9 talc = 5 protoanthophyllite + 4 H_2O, or by inversion from anthophyllite produced by 4 forsterite + 9 talc = 5 anthophyllite + 4 H_2O (Konishi et al. 2002).

The physical and optical properties of protoanthophyllite are summarized in Table 2. Protoanthophyllite is biaxial negative and the refractive indices n_α = 1.593(2), n_β (calc.) = 1.609, n_γ = 1.615(2), and $2Vx$ = 64(5)°. Most properties are similar to those of anthophyllite. The formula, based on the data in Table 3, is $(Mg_{6.31}Fe_{0.61}Na_{0.06}Mn_{0.01}Ni_{0.01})_{\Sigma 7.00}(Si_{7.90}Al_{0.14})_{\Sigma 8.04}O_{22}(OH)_2$. No F and Cl were detected using wavelength-dispersive X-ray spectroscopy.

TABLE 2. Physical and optical properties of protoanthophyllite

Morphology	Prismatic, elongated along *c*-axis
Color	Colorless in thin section
Luster	Vitreous
Streak	White
Cleavage	Perfect {110}
Tenacity	Brittle
Fracture	Uneven
Twining	Not observed
Hardness	Mohs approximately 6
Density (calc.)	2.98 g/cm^3
Optical characters	Biaxial
Optical sign	X = a, Y = b, and Z = c
Indices of refraction	α = 1.593(2)
	β (calc.) = 1.609
	γ = 1.615(2)
2V	64(5)
Orientation	Negative
Elongation	Positive
Pleochroism	Not observed

Notes: Luster, streak, tenacity, fracture, hardness, indices of refraction, and elongation were obtained by S.M. and the others by H.K. Microhardness was measured on a randomly oriented surface using an Akashi MVK microhardness tester, and the corresponding Mohs hardness was estimated.

DESCRIPTION OF THE STRUCTURE AND DISCUSSION

Tables 4 through 8[1] present the fractional coordinates, anisotropic displacement parameters, selected interatomic distances and angles, observed and calculated structure factors, and powder X-ray diffraction data. Comparison of the refined protoanthophyllite structure with protoferro-anthophyllite, protomangano-ferro-anthophyllite (Sueno et al. 1998), protofluorian-lithian-anthophyllite (Gibbs 1969), and anthophyllite (Finger 1970) structures reveals some notable features.

TABLE 3. Composition of protoanthophyllite

	wt%	Range	SD
SiO_2	58.53	58.37–58.86	0.28
TiO_2	0.01	0.00–0.01	0.01
Al_2O_3	0.87	0.75–0.95	0.11
Cr_2O_3	0.02	0.00–0.04	0.02
FeO	5.43	5.17–5.72	0.28
MnO	0.12	0.11–0.13	0.01
NiO	0.11	0.11–0.11	0.00
MgO	31.33	31.13–31.44	0.18
CaO	0.01	0.00–0.02	0.01
Na_2O	0.24	0.17–0.29	0.06
K_2O	0	0.00–0.01	0.01
H_2O (Calc.)	2.22		
Total	98.9		

Number of ions on the basis of 23 O atoms	
Si	7.90
Al	0.14
T sites	8.04
Mg	6.31
Fe	0.61
Mn	0.01
Ni	0.01
M sites	6.94
Na	0.06
A site	0.06

Notes: The average composition of three analyses. SD = standard deviation.

Protoanthophyllite is a polymorph of anthophyllite [$(Mg,Fe)_7Si_8O_{22}(OH)_2$] and isostructural with synthetic protofluorian-lithian-anthophyllite, natural protoferro-anthophyllite, and protomangano-ferro-anthophyllite. As shown in Figures 1a and b, the octahedra change their orientations in successive layers, thus following the proto-stacking (X) sequence.

The M1, M2, and M3 octahedra in protoanthophyllite are nearly regular, with mean M-O bond lengths of 2.093, 2.078, and 2.073 Å, respectively. They are smaller than those of protoferro-anthophyllite (2.126, 2.133, and 2.114 Å) and protomangano-ferro-anthophyllite (2.133, 2.122, and 2.113 Å). A result is that the silicate tetrahedral chain is more kinked in protoanthophyllite [$\angle$O5-O6-O5 = 170.06(10)°] than in Fe- and Mn-rich species [$\angle$O5-O6-O5 = 177.2°]. The O5-O6-O5 angle indicates the extent to which the tetrahedral chain is kinked (Fig. 1c). If the chain is straight, the angle is 180°.

The O6-O7-O6 and O5-O7-O5 angles also indicate the topology of the double chain. These angles in protoanthophyllite are 129.00(12)° and 110.09(11)°, respectively (Fig. 1c), whereas those for the straight double chains are 120°. The topology of

[1] For a copy of Table 7, deposit item AM-03-042, contact the Business Office of the Mineralogical Society of America (see inside front cover of recent issue) for price information. Deposit items may also be available on the American Mineralogist web site at http://www.minsocam.org.

TABLE 4. Atomic coordinates, equivalent isotropic displacement parameters, and site occupancies

Atom	*x*	*y*	*z*	U_{eq}	Site ocupancy
M1	0	0.08724(6)	0.5	0.0067(3)	0.9788(9) Mg 0.0212(9) Fe
M2	0	0.17748(6)	0	0.0066(2)	1.0000(7) Mg
M3	0	0	0	0.0083(4)	0.9749(9) Mg 0.0251(10) Fe
M4	0	0.25991(5)	0.5	0.0085(2)	0.7226(9) Mg 0.2773(9) Fe
T1	0.28464(7)	0.08483(3)	0.17327(13)	0.00548(14)	0.9971(8) Si 0.0040(7) Al
T2	0.29399(6)	0.17095(3)	0.67034(13)	0.00632(14)	0.9928(8) Si 0.0080(7) Al
O1	0.11279(17)	0.08668(8)	0.1666(3)	0.0084(4)	O
O2	0.12137(17)	0.17464(9)	0.6699(3)	0.0091(4)	O
O3	0.1128(2)	0	0.6656(4)	0.0090(5)	O
O4	0.1211(18)	0.25265(9)	0.1834(4)	0.0093(4)	O
O5	0.34360(17)	0.11987(9)	0.4330(3)	0.0118(4)	O
O6	0.34888(17)	0.13244(9)	0.9374(3)	0.0122(4)	O
O7	0.3414(2)	0	0.1502(5)	0.0102(6)	O
H	0.225(5)	0	0.682(9)	0.036(14)	H
A	0.5	0	0.5	0.05(2)	0.048(3) Na

Note: Site nomenclature used for protoanthophyllite is identical to that used by Hawthorne (1981).

TABLE 5. Anisotropic displacement parameters (Å^2)

Atom	U_{11}	U_{22}	U_{33}	U_{23}	U_{13}	U_{12}
T1	0.0052(3)	0.0053(3)	0.0060(3)	0.0003(2)	–0.0001(3)	–0.0003(2)
T2	0.0058(3)	0.0065(3)	0.0066(3)	–0.0001(3)	0.0001(3)	–0.0009(2)
M1	0.0087(5)	0.0048(5)	0.0068(5)	0.000	–0.0002(5)	0.000
M2	0.0067(5)	0.0064(5)	0.0068(5)	0.000	0.0003(5)	0.000
M3	0.0092(7)	0.0074(7)	0.0083(7)	0.000	–0.0012(7)	0.000
M4	0.0096(4)	0.0090(4)	0.0070(4)	0.000	–0.0020(4)	0.000
O1	0.0090(8)	0.0081(8)	0.0083(8)	–0.0003(7)	0.0010(7)	0.0007(6)
O2	0.0116(7)	0.0072(7)	0.0083(8)	0.0002(7)	–0.0005(7)	–0.0009(6)
O3	0.0076(10)	0.0089(11)	0.0104(11)	0.000	0.0004(11)	0.000
O4	0.0116(8)	0.0064(7)	0.0099(9)	–0.0001(7)	0.0005(7)	–0.0022(6)
O5	0.0101(8)	0.0138(9)	0.0115(9)	–0.0051(7)	–0.0016(7)	0.0005(7)
O6	0.0088(8)	0.0151(8)	0.0125(9)	0.0049(7)	–0.0001(7)	–0.0005(7)
O7	0.0068(10)	0.0079(11)	0.0158(13)	0.000	0.0019(11)	0.000

TABLE 6. Selected interatomic distances and angles

Atoms	Distances Å	Atoms	Distances Å
T1 tetrahedron		Octahedra	
T1-O1	1.6084(17)	M1-O1	2.0615(16)
T1-O5	1.6132(18)	M1-O2	2.1353(17)
T1-O6	1.6310(18)	M1-O3	2.0819(17)
T1-O7	1.6157(10)	M1-O	2.093
T-O	1.617		
		M2-O1	2.1324(18)
O1-O5	2.649(2)	M2-O2	2.0896(16)
O1-O6	2.652(2)	M2-O4	2.0123(17)
O1-O7	2.646(2)	M2-O	2.078
O5-O6	2.643(2)		
O5-O7	2.622(2)	M3-O1	2.0766(16)
O6-O7	2.631(2)	M3-O3	2.066(2)
O-O	2.641	M3-O	2.073
T2 tetrahedron		M4-O2	2.1073(17)
T2-O2	1.6163(17)	M4-O4	2.0319(16)
T2-O4	1.5851(17)	M4-O6	2.4156(18)
T2-O5	1.6259(17)		
T2-O6	1.6591(18)		
T2-O	1.622		
O2-O4	2.740(2)		
O2-O5	2.621(2)		
O2-O6	2.669(2)		
O4-O5	2.665(2)		
O4-O6	2.479(2)		
O5-O6	2.689(2)		
O-O	2.644		

Angles (°)		Angles (°)	
T1 tetrahedron		Octahedra	
O1-T1-O5	110.64(9)	O1-M1-O2	95.42(7)
O1-T1-O6	109.91(9)	O1-M1-O2	84.99(6)
O1-T1-O7	110.27(10)	O1-M1-O3	95.73(8)
O5-T1-O6	109.10(9)	O1-M1-O3	83.85(8)
O5-T1-O7	108.60(11)	O2-M1-O2	85.57(9)
O6-T1-O7	108.26(11)	O3-M1-O3	82.57(10)
		O2-M1-O3	95.94(6)
T2 tetrahedron			
O2-T2-O4	117.73(9)	O1-M2-O1	80.45(9)
O2-T2-O5	107.89(9)	O1-M2-O2	93.48(7)
O2-T2-O6	109.12(9)	O1-M2-O2	84.38(6)
O4-T2-O5	112.20(9)	O1-M2-O4	91.82(6)
O4-T2-O6	99.61(9)	O2-M2-O4	96.70(7)
O5-T2-O6	109.88(9)	O2-M2-O4	85.18(7)
		O4-M2-O4	95.90(10)
Chains			
T1-O5-T2	141.71(11)	O1-M3-O1	96.92(9)
T1-O6-T2	139.52(11)	O1-M3-O1	83.08(9)
T1-O7-T1	140.56(16)	O1-M3-O3	96.14(6)
		O1-M3-O3	83.86(6)
O5-O6-O5	170.06(10)		
O5-O7-O6	170.31(11)	O2-M4-O4	90.43(7)
O5-O7-O5	110.09(11)	O2-M4-O6	108.86(6)
O6-O7-O6	129.00(12)	O4-M4-O6	119.44(7)
		O6-M4-O6	73.92(8)
		O2-M4-O4	84.23(6)
		O2-M4-O2	86.98(9)
		O4-M4-O6	67.10(6)

TABLE 9. Selected interatomic angles

	O5-O6-O5	O5-O7-O5	O6-O7-O6
protoanthophyllite	170.06(10)	110.09(11)	129.00(12)
protoferro-anthophyllite	177.2	122.2	115.9
protomangano-ferro-anthophyllite	178.6	118.5	120.2
protofluorian-lithian-anthophyllite	173.1	113.8	125.0
anthophyllite (A-chain)	169.2	130.2	109.9

Notes: Anthophyllite O5 and O6 correspond to protoamphibole O6 and O5, respectively.The O-O-O angles were calculated from published data (Gibbs 1969; Sueno et al. 1998; Finger 1970) and the present study.

TABLE 8. X-ray powder-diffraction data for protoanthophyllite

h k l	*I* (obs)	*d* (obs)	*d* (calc)	*I* (calc)
0 2 0	21	8.97	8.98	34
1 1 0	71	8.32	8.30	77
0 1 1	9	5.10	5.10	8
1 3 0			5.04	5
2 0 0			4.68	6
1 0 1	10	4.62	4.62	7
0 4 0	26	4.48	4.49	24
1 1 1			4.48	24
2 2 0	10	4.15	4.15	10
0 3 1	6	3.98	3.98	5
1 3 1	100	3.66	3.66	81
2 2 1	49	3.27	3.27	37
2 4 0	37	3.24	3.24	48
3 1 0	81	3.08	3.08	78
2 3 1	22	3.03	3.03	19
1 5 1	96	2.84	2.84	100
3 3 0	20	2.77	2.77	18
3 2 1			2.58	14
1 0 2	49	2.56	2.56	52
1 6 1	57	2.51	2.51	18
2 5 1			2.51	47
2 0 2	36	2.31	2.31	42
2 1 2			2.29	6
2 6 1	17	2.28	2.28	13
1 7 1	14	2.243	2.244	22
2 3 2	6	2.157	2.157	3
4 2 1	12	2.083	2.084	9
2 7 1			2.072	5
3 1 2			2.012	9
3 6 1	30	2.002	2.002	34
1 9 0			1.952	2
2 5 2	3	1.944	1.944	3
5 1 0	8	1.863	1.863	7
3 4 2			1.845	6
4 5 1	15	1.841	1.840	9
1 9 1			1.832	11
5 3 0	4	1.785	1.788	3
4 0 2	8	1.757	1.757	8
4 1 2			1.749	5
4 6 1	14	1.743	1.742	15
0 8 2			1.715	4
1 2 3	6	1.712	1.710	4
0 3 3	7	1.700	1.700	8
1 8 2	9	1.688	1.687	7
4 4 2	12	1.636	1.636	10
1 11 0			1.608	10
0 5 3	25	1.589	1.590	25
6 0 0			1.561	5
5 1 2			1.526	11
5 6 1	40	1.522	1.522	33
1 6 3	26	1.505	1.505	19
0 12 0			1.497	15
0 7 3	8	1.458	1.458	6
5 4 2	7	1.448	1.449	4
3 11 0			1.447	3
6 5 1	7	1.382	1.382	7
1 11 2			1.376	5
3 6 3	12	1.370	1.370	9
6 0 2	6	1.358	1.346	7
6 1 2			1.342	7
6 6 1	26	1.339	1.340	19
1 0 4	14	1.316	1.316	12
1 12 2	8	1.292	1.292	16
2 0 4	6	1.276	1.279	5
5 2 3			1.275	3

Notes: The X-ray powder diffraction pattern of a lamella-free fragment was recorded in vacuum using a Gandolfi camera with a camera length of 114.6 mm, Ni-filtered, Cu$K\alpha$ radiation (30 kV, 20 mA), and a three-day exposure time. The data were recorded on an imaging plate, processed with a Fuji BAS-2500 bio-image analyzer, and reduced using the program of Nakamuta (1999). The reflections were indexed using the results of the single-crystal study. The intensity of the 442 reflection was determined using an external Si-standard (NBS no. 640b), whereas the others were determined using an internal Si-standard. Refinement of the powder-diffraction data gave an orthorhombic cell with a = 9.366(2), b = 17.959(5), and c = 5.318(1) Å; V = 894.5(4) Å^3, using a computer program of Toraya (1993). The calculated pattern was obtained using Cerius 2 (Molecular Simulation Inc.)

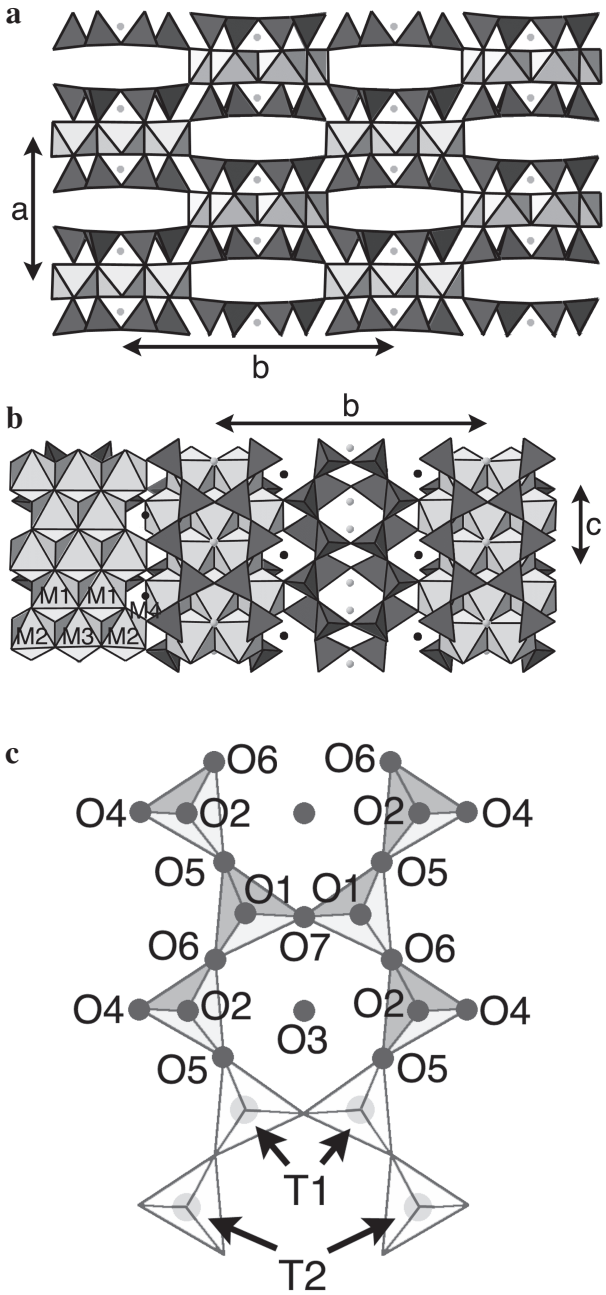

FIGURE 1. Protoanthophyllite structure viewed along the (**a**) **c**- and (**b**) **a**-axes. (**c**) Silicate tetrahedral chains and atomic site nomenclature of O- and Si-atom positions. Also see the site nomenclature in Table 4. The small, light-gray balls denote H atoms in **a** and **b**, and the small, black balls indicate atoms on M4 sites in (**b**). Triangles and rectangles composed of triangles represent SiO_4 tetrahedra and MO_6 octahedra, respectively.

the tetrahedral chains in protoanthophyllite is similar to that of the anthophyllite A-chain (Table 9). The silicate tetrahedral chains in protoanthophyllite, as in anthophyllite and protofluorian-lithian-anthophyllite, are O-rotated whereas those in protomangano-ferro-anthophyllite and protoferro-anthophyllite are nearly ideal and slightly S-rotated, respectively.

Atoms on the M4 site in protoanthophyllite are 4-coordinated as in protoferro-anthophyllite and protomangano-ferro-anthophyllite, based on the calculation of the bond critical-point properties of the electron density distribution (Sueno et al. 1998; Gibbs, personal communication). The M4-O6 distance of protoanthophyllite [2.4156(18) Å], however, is much shorter than that of protoferro-anthophyllite and protomangano-ferro-anthophyllite [2.671(2) and 2.582(3) Å, respectively].

It is not known whether protoanthophyllite has a stability field in the MgO-FeO-SiO_2-H_2O system. Protoanthophyllite has not been recognized in synthesized anthophyllite samples; however, protoanthophyllite could have been misidentified as anthophyllite because of their similarity in optical properties and powder X-ray patterns (Konishi et al. 2002). It is possible that protoanthophyllite has a true stability field because it occurs in three different metamorphosed serpentinites (Konishi et al. 2002). It is also possible that protoanthophyllite may occur unrecognized in the experimental runs used to determine the anthophyllite phase relations. In that event, the stability field of protoanthophyllite may overlap with that reported for anthophyllite.

The observed unit-cell volume of the protoanthophyllite [a = 9.3553(8), b = 17.9308(15), c = 5.3117(4) Å; V = 891.0(3) Å^3] with Mg/(Mg + Fe) = 0.9 is 1.5 % larger than that reported for anthophyllite with Mg/(Mg + Fe) = 0.885 (Evans et al. 2001), suggesting that protoanthophyllite is a high-temperature or low-pressure form of anthophyllite. Based on the mineral assemblages and metamorphic zonation described by previous workers (Evans and Trommsdorff 1970; Matsumoto et al. 1995), we conclude that protoanthophyllite likely formed by reaction between forsterite and talc during contact metamorphism.

The refined structure of protoanthophyllite indicates that Fe atoms are concentrated in M4 sites. Such a high degree of cation ordering in the M sites also occurs in anthophyllite, indicating annealing at a relatively low temperature (Finger 1970; Seifert 1978; Evans et al. 2001). Such low-temperature ordering can result from thermal metamorphism by the intrusion of granitic rocks and the very slow cooling history that is generally expected as such intrusives cool.

A direct demonstration of the growth of one phase relative to another is the best way to define the stability field of a given polymorph (Jenkins, personal communication). Because we can now recognize and distinguish protoanthophyllite from anthophyllite, we should be able to investigate the relative stability of these two polymorphs in subsequent experimental studies.

ACKNOWLEDGMENTS

We thank Craig L. Johnson, Thomas J. Zega, Laurence A. J. Garvie, David M. Jenkins, Eugene A. Smelik, Kiyoshi Ishida, Katsutoshi Tomita, Bernard W. Evans, and James B. Thompson for useful discussion and comments. Critical reviews by Gerry V. Gibbs and an anonymous reviewer were very useful for improving the paper. Funding was provided by NSF grant EAR 0003533.

REFERENCES CITED

Evans, B.W. and Trommsdorff, V. (1970) Regional metamorphism of ultramafic rocks in the Central Alps: Parageneses in the system CaO-MgO-SiO_2-H_2O. Schweizerische Mineralogische und Petrographische Mitteilungen, 50, 481–492.

Evans, B.W., Ghiorso, M.S., Yang, H., and Medenbach, O. (2001) Thermodynamics of the amphiboles: Anthophyllite-ferroanthophyllite and the ortho-clino phase loop. American Mineralogist, 86, 640–651.

Finger, L.W. (1970) Refinement of the crystal structure of an anthophyllite. Year Book Carnegie Institution of Washington, 283–288.

Gibbs, G.V. (1969) Crystal structure of protoamphibole. Pyroxenes and amphiboles—Crystal chemistry and phase petrology. Mineralogical Society of America, Special paper 2, 101–109.

Gibbs, G.V., Bloss, F.D., and Shell, H.R. (1960) Proto-amphibole, a new polytype. American Mineralogist, 45, 974–989.

Hawthorne, F.C. (1981) Crystal chemistry of the amphiboles. In D.R. Veblen, Ed. Amphiboles and other hydrous pyriboles—mineralogy, 9A, p. 1–102. Reviews in Mineralogy, Mineralogical Society of America, Washington, D.C.

Konishi, H., Dódony, I., and Buseck, P.R. (2002) Protoanthophyllite from three metamorphosed serpentinites. American Mineralogist, 87, 1096–1103.

Leake, B.E., Woolley, A.R., Arps, C.E.S., Birch, W.D., Gilbert, M.C., Grice, J.D., Hawthorne, F.C., Kato, A., Kisch, H.J., Krivovichev, V.G., Linthout, K., Laird, J., Mandarino, J.A., Maresch, W.V., Nickel, E.H., Rock, N.M.S., Schumacher, J.C., Smith, D.C., Stephenson, N.C.N., Ungaretti, L., Whittaker, E.J.W., and Youzhi, G. (1997) Nomenclature of amphiboles: Report of the Subcommittee on Amphiboles of the International Mineralogical Association, Commission on New Minerals and Mineral Names. American Mineralogist, 82, 1019–1037.

Matsumoto, I., Arai, S., Muraoka, H., and Yamauchi, H. (1995) Petrological characteristics of the dunite-harzburgite-chromite complexes of Sangun zone, Sowthwest Japan (in Japanese). Journal of the Japanese Association of Mineralogists, Petrologists and Economic Geologists, 90, 13–26.

Nakamuta, Y. (1999) Precise analysis of a very small mineral by an X-ray diffraction method (in Japanese). Journal of the Mineralogical Society of Japan, 28, 117–121.

Seifert, F. (1978) Equilibrium Mg-Fe^{2+} cation distribution in anthophyllite. American Journal of Science, 278, 1323–1333.

Sheldrick, G.M. (1997a) SHELXL97. Program for the refinement of crystal structures. University of Göttingen, Germany.

———(1997b) SHELXS97. Program for the solution of crystal structures. University of Göttingen, Germany.

Smith, J.V. (1959) The crystal structure of proto-enstatite, $MgSiO_3$. Acta Crystallographica, 12, 515–519.

Sueno, S., Matsuura, S., Gibbs, G.V., and Boisen, M.B., Jr. (1998) A crystal chemical study of protoanthophyllite: orthoamphiboles with the protoamphibole structure. Physics and Chemistry of Minerals, 25, 366–377.

Thompson, J.B. Jr. (1970) Geometrical possibilities for amphibole structures: model biopyriboles. American Mineralogist, 55, 292–293.

———(1981) An introduction to the mineralogy and petrology of the biopyriboles. In D.R. Veblen, Ed. Amphiboles and other hydrous pyriboles—mineralogy, 9A, p. 141–188. Reviews in Mineralogy, Mineralogical Society of America, Washington, D.C.

Toraya, H. (1993) The determination of unit-cell parameters from Bragg reflection data using a standard reference material but without a calibration curve. Journal of Applied Crystallography, 26, 583–590.

MANUSCRIPT RECEIVED MARCH 10, 2002
MANUSCRIPT ACCEPTED JULY 17, 2003
MANUSCRIPT HANDLED BY ADRIAN J. BREARLEY